Journal of Power Sources 180 (2008) 724–732

Contents lists available at ScienceDirect

Journal of Power Sources

journal homepage: www.elsevier.com/locate/jpowsour

Cathode catalyst layer using supported Pt catalyst on ordered mesoporous carbon for direct methanol fuel cell

Hee-Tak Kim[a,*], Dae Jong You[b], Hae-Kwon Yoon[a], Sang Hoon Joo[b], Chanho Pak[b], Hyuk Chang[b], In-Seob Song[a]

[a] Samsung SDI Co. Ltd., 575 Shin-dong, Yeongtong-gu, Suwon-si, Gyeonggi-do 443-391, Republic of Korea
[b] Samsung Advanced Institute of Technology, P.O. Box 111, Suwon 440-600, Republic of Korea

ARTICLE INFO

Article history:
Received 30 October 2007
Received in revised form 13 December 2007
Accepted 11 February 2008
Available online 7 March 2008

Keywords:
Fuel cell catalyst
Membrane electrode assembly
Direct methanol fuel cell
Ordered mesoporous carbon
Agglomerate
Power density

ABSTRACT

The development of a cathode catalyst layer based on a supported Pt catalyst using an ordered mesoporous carbon (OMC) for direct methanol fuel cell is reported. An OMC with a mesopore structure between hexagonally arranged carbon nanorods is prepared using a template method. Platinum nanoparticles are supported on the OMC (Pt/OMC) with high metal loading of 60 wt.%. Compositional and morphological variations are made by varying the ionomer content and by compressing the catalyst layer to detect a parameter that determines the power performance. Increase in power density with decrease in the volume fraction of ionomer in the agglomerate comprising the Pt/OMC and the ionomer indicates that mass transport through the ionomer phase governs the kinetics of oxygen reduction. Impedance spectroscopic analysis suggests that a significant mass-transport limitation occurs at high ionomer content and in the compressed cathode. The power density of the optimum cathode layer, which employs a Pt/OMC catalyst with a Pt loading of 2 mg cm^{-2}, is greater than that of a catalyst layer with 6 mg cm^{-2} Pt-black catalyst at a voltage higher than 0.4 V. This would lead to a significant reduction in the cost of the membrane electrode assembly.

1. Introduction

Recently, novel nanostructured carbon materials have attracted much interest as electrocatalyst supports for fuel cell applications because of their excellent electrical and mechanical properties. The examples are supports produced from carbon nanofibres [1–4], carbon nanotubes [5–7], carbon aerogels [8–11] and ordered mesoporous carbons (OMCs) [12–17]. Among these nanostructured carbons, OMCs are highly intriguing as carbon supports for fuel cell application on account of their ordered pore structure. The OMC is constructed of periodic arrays of carbon nanorods or nanopipes, with uniform mesopores existing between them.

The performance of the catalyst layer is generally dependent on its compositional and morphological characteristics and on the optimization of properties such as catalyst loading, ionomer content and porosity in conjunction with the structure of the catalyst employed. Intensive research has been devoted to optimization of the structure and composition of the catalyst layer [18–32]. Some studies have focused on the effects of ionomer loading [18–28]. Addition of Nafion® (a proton-conducting ionomer) to the catalyst layer enhances fuel cell performance due to increased proton transport through the catalyst layer and increased catalyst utilization. Above a certain amount of ionomer, the cell performance often decreases, which is attributed to mass-transport limitation by the thick ionomer phase covering the catalysts or to an increase in resistance by non-electronic conductive ionomers in the catalyst layer. Ionomer loading depends mostly on the catalyst type: black or supported [28]. Compared with unsupported catalyst, supported catalysts generally require considerably higher amounts of ionomer [28]. Also, the supported catalyst generates a thicker catalyst layer although it has the same amount of catalyst loading on the membrane electrode assembly (MEA) as that of the black catalyst based on the weight of active metal, which is attributed to the large volume of the supporting material.

The present study deals with the development of a cathode catalyst layer based on a supported Pt catalyst on OMC (Pt/OMC) for application in a direct methanol fuel cell (DMFC). This considers a balance between proton conduction and mass transport through the catalyst layer. Compositional and morphological variations are made by varying ionomer content and by compressing the catalyst layer. Current–voltage behaviour and electrochemical impedance are investigated for the catalyst layers. An attempt is made to determine which structural parameter of the catalyst layer governs power performance. In addition, the power performance of

* Corresponding author. Tel.: +82 31 210 7047; fax: +82 31 210 7374.
E-mail address: hee-tak.kim@samsung.com (H.-T. Kim).

0378-7753/$ – see front matter © 2008 Elsevier B.V. All rights reserved.
doi:10.1016/j.jpowsour.2008.02.081

the optimized Pt/OMC cathode is compared with that of a cathode based on unsupported Pt-black catalyst to explore the possibility of reducing the amount of Pt without loss in the power performance of a DMFC.

2. Experimental

2.1. Synthesis of ordered mesoporous silica and carbon

Hexagonally ordered mesoporous silica (OMS) with large pores was used as a template for the synthesis of OMC. The synthesis of OMS was performed via the method reported previously [17], which used Pluronic P123 triblock copolymer as a supramolecular template and sodium silicate as a silica source under near-neutral conditions. P123 triblock copolymer and sodium silicate solution of Na/Si = 2.5 (10 wt.% SiO_2) were mixed in de-ionized water, followed by the addition of acetic acid solution to neutralize the mixture and polymerize the silicate species. The gel mixture was stirred at 45 °C for 20 h and placed in an oven at 100 °C for 24 h under static conditions. The silica precipitate was filtered, washed with distilled water, and dried in an oven. The product was finally calcinated in static air at 550 °C for 3 h.

From the above-synthesized OMS template, the hexagonally ordered OMC was replicated using phenanthrene precursors. The synthesis of OMC derived from phenanthrene has been reported elsewhere [17]. The carbon precursor solution was prepared by dissolving a 0.7 g of phenanthrene and 2.1 g of *p*-toluenesulfonic acid in 7 ml of acetone. The precursor solution was divided into three portions. After impregnating the precursor solution into 1 g of OMS template using an incipient wetness method, the mixture was dried at 100 °C and subsequently at 160 °C. The impregnation-drying step was repeated twice to completely infiltrate the internal pores of OMS template with carbon sources. The mixture was then carbonized by heating to 1100 °C under nitrogen flow for 2 h. Finally, the silica templates were dissolved at room temperature using 10% HF in de-ionized water–ethanol solution.

2.2. Preparation of OMC-supported Pt catalyst

A 0.5 g sample of OMC was mixed with 1.5 ml of acetone solution containing $H_2PtCl_6{\cdot}xH_2O$ (Umicore) using an incipient wetness method. The amount of $H_2PtCl_6{\cdot}xH_2O$ in the solution was controlled to obtain a metal loading of 60 wt.%. After being dried overnight in an oven at 60 °C, the impregnated OMC material was heated in a hydrogen flow to 200 °C and kept for 2 h at the same temperature. The adsorbed hydrogen was removed by heating to 350 °C and kept for 2 h under nitrogen flow. The sample thus prepared was denoted as Pt/OMC. The size of the Pt particles was measured from the X-ray diffraction (XRD) patterns obtained using a Philips X'pert Pro X-ray diffractometer equipped with a Cu Kα source at 40 kV and 30 mA. Transmission electron microscope (TEM) images were taken with a G2 FE-TEM Tecnai microscope at an accelerating voltage of 200 kV. Scanning electron microscope (SEM) images were obtained with a Hitachi S-4500 field emission scanning electron microscope at 20 kV.

2.3. Preparation of catalyst layer based on Pt/OMC

Pt/OMC and PtRu black (Johnson Matthey, Hispec 6000) were used as catalysts for the cathode and the anode, respectively. Cathode catalyst ink, consisting of appropriate amounts of Pt/OMC catalyst, Nafion® solution (5 wt.%, 1100 EW, DuPont) and isopropyl alcohol, was homogenized to disperse the catalyst. The weight ratio of the ionomer and Pt/OMC catalyst (R_I) (dry weight) was varied as 0.12, 0.18, 0.30 and 0.45. The slurry with the unsupported PtRu catalyst for the anode catalyst layer was prepared in the same manner. The weight ratio of the ionomer and PtRu black catalyst was maintained at 0.12, irrespective of the cathode composition.

The catalyst ink was sprayed directly on to a Nafion® 115 membrane to form a so-called catalyst coated membrane (CCM). The membrane was held on a vacuum plate to prevent dimensional change of the membrane during the direct coating of the ink. The cathode catalyst ink was coated on one side of the membrane followed by drying at 60 °C under vacuum for 2 h. On the uncoated side of the cathode-coated membrane, the anode catalyst ink was applied in the same manner. The Pt loading (LL_{Pt}) for the cathode and the anode was around 2 and 6 mg cm^{-2}, respectively. As a reference, the catalyst layer based on unsupported Pt-black (Johnson Matthey, Hispec 1000) at a loading level of 6 mg cm^{-2} was also prepared. The geometric area of the catalyst layers was 25 cm^2.

In order to produce a catalyst layer with lower porosity, the cathode-coated membranes were compressed at 30 MPa and at 135 °C for 5 min before the subsequent anode coating was performed. As a diffusion layer, 35 BC (SGL, Germany) was used for both the cathode and the anode. The MEAs were prepared by pressing the CCM and two diffusion layers at 125 °C and at 51 MPa. The morphology of the catalyst layers was observed by means of SEM.

2.4. Electrochemical characterization

The MEAs were sandwiched between two plates with triple serpentine flow channels and then mechanically pressed, to ensure a tight seal. An electrical heater and thermocouple were embedded in the plates for temperature control. One molar aqueous methanol solution was pumped to the anode side at a stoichiometry of 3. Ambient air was fed by a pump into the cathode side at a stoichiometry of 3 and at ambient back-pressure. The MEAs were conditioned by operation at 0.4 V and at 50 °C for 2 h. After the conditioning, *I–V* polarization was successively obtained at 50, 60 and 70 °C. This process was repeated for 7 days. The power performance was generally increased and stabilized within the first 5 days. A further test for two more days did not cause any change in performance. The *I–V* polarizations measured at the fifth day are presented in this study.

Electrochemical impedances of the MEAs were recorded with a IM6 system (Zahner, Germany) at 70 °C in the frequency range from 10 kHz to 0.1 Hz. The impedances were measured under galvanostatic control. The amplitude of the sinusoidal voltage signal was set at 5 mV. In order to separate anode and cathode impedances from the total cell impedance, the anode impedance produced by the injection of hydrogen into the cathode compartment was measured. By subtracting the anode impedance from the total cell impedance, cathode impedance can be extracted [33,34].

The double-layer capacitance of the cathode catalyst layer was measured using a cyclic voltammetry technique [27]. The double-layer capacitance was calculated from the change in the capacitive current with scan rate. The working electrode compartment (cathode) was supplied with fully humidified nitrogen, whereas the counter and reference electrode compartments (anode) were fed with fully humidified hydrogen, which acted as dynamic hydrogen electrode (DHE). The potential was scanned from 0.09 to 0.8 versus DHE at 60 °C with sweep rates of 20, 50, 80 and 100 mV s^{-1}.

3. Results and discussion

3.1. Characterization of Pt/OMC catalyst

The morphology and pore structure of OMS and OMC were examined by means of SEM and TEM, respectively, as shown in Fig. 1. The SEM image in Fig. 1(a) shows that OMS is composed of 200–300 nm spherical particles. As seen in Fig. 1(b), OMC exhibits

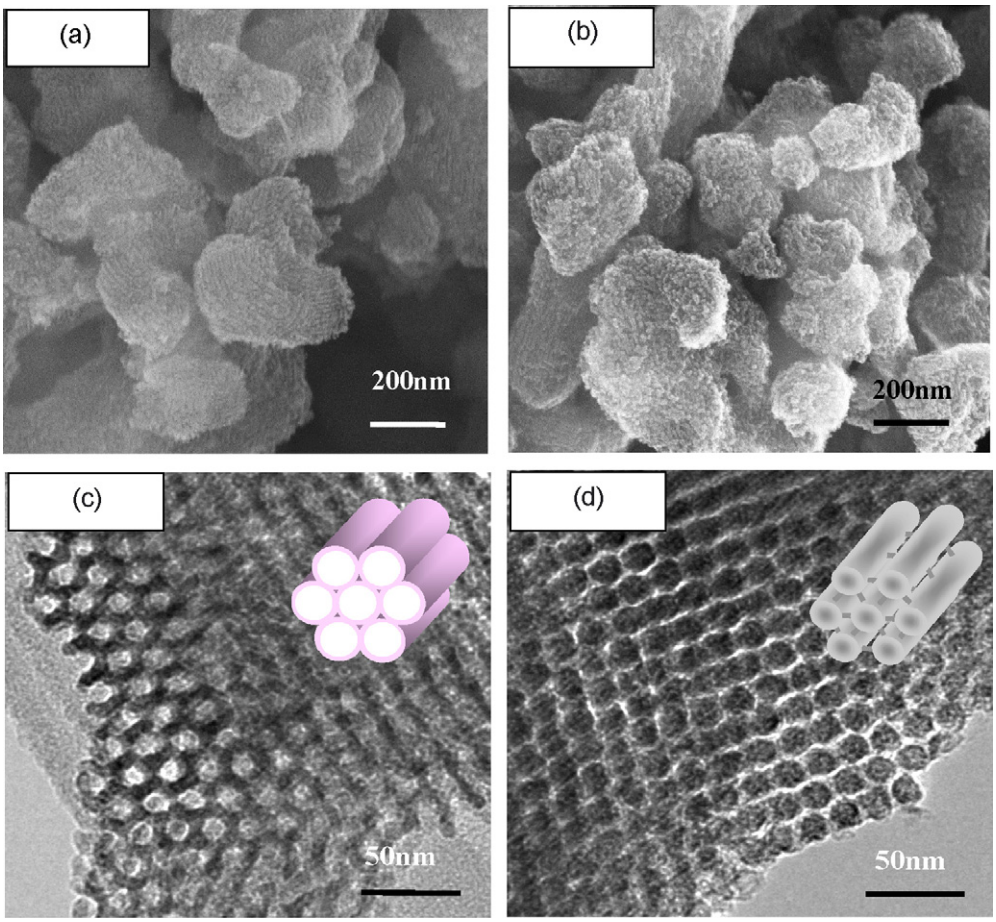

Fig. 1. SEM images of (a) OMS and (b) OMC, and TEM images of (c) OMS and (d) OMC.

similar particle morphology and size and this indicates that the particle shape was maintained during the carbonization and subsequent removal of the OMS template without any significant modification or alternation. The internal pore structures of OMS and OMC were observed with TEM, as shown in Fig. 1(c) and (d), respectively. The TEM image for OMS (Fig. 1(c)) reveals that uniform mesopores are periodically arranged along and perpendicular to the direction of the hexagonal pore arrangement. The TEM image of OMC in Fig. 1(d) clearly reveals that the pore structure of the carbon is an exactly inverse replica of OMS, in that the pores and the walls of OMS are converted to carbon nanorods and mesopores of OMC, respectively.

The structure of Pt/OMC was characterized with TEM and XRD techniques. The TEM image of Pt/OMC (Fig. 2(a)) indicates that Pt nanoparticles are uniformly produced on the surface of OMC. The mean diameter determined from the TEM image is 2.85 nm. The XRD patterns for 60 wt.% Pt-loaded OMC (Pt/OMC) presented in Fig. 2(b) exhibit distinct peaks at around 39.8, 46.3 and 67.5, which correspond to the (1 1 1), (2 0 0) and (2 2 0) planes of a face-centered cubic structure, respectively. The average particle size of the catalysts estimated by means of the Debye–Scherrer equation is 2.86 nm, i.e., a value which is in good agreement with that estimated from TEM analysis.

3.2. Structural characteristics of Pt/OMC-based catalyst layers

The characteristics of the catalyst layers studied in this work are listed in Table 1. M18-U, M30-U and M45-U are the uncompressed catalyst layers, in which the ionomer contents are 0.18, 0.30 and 0.45, respectively. M18-C, M30-C and M45-C were prepared by the compression of M18-U, M30-U and M45-U, respectively. The thickness of the uncompressed catalyst layers is 70, 128 and 132 μm for corresponding ionomer contents of 0.18, 0.30 and 0.45. The thickness of the compressed cathode was found to be 64, 53 and 48% of the original thickness for ionomer contents of 0.18, 0.30 and 0.45, respectively. At an ionomer content of 0.12, the mechanical integrity of the catalyst layer is poor. This is attributed to the fact that the ionomer content is inadequate to bind Pt/OMC catalysts effectively. At ionomer contents higher than 0.12, the catalyst layers reveal acceptable mechanical integrity and are therefore used for MEA preparation.

The morphology of the Pt/OMC-based catalyst layers was observed with SEM, as shown in Fig. 3. These are featured by the formation of agglomerates of the Pt/OMC and ionomer and of pores between these agglomerates. The agglomerate size is in the range of 200–1000 nm. Considering that the size of the pristine OMC is 200–300 nm, several Pt/OMC particles are included in the agglomerate. The variation of ionomer content does not cause an appreciable change in the size of the agglomerates. For the uncompressed catalyst layers, the porosity appears to be larger at higher ionomer contents. After compression, densification of the catalyst layer is observed. On the other hand, the size of the agglomerates is little affected by the compression, as shown in Fig. 3. This indicates that macropores between the agglomerates are reduced during the compression process. The compressed catalyst layers do not differ in their pore structures.

In order to identify fundamental parameters that determine the power performance of the Pt/OMC-based catalyst layer, an analy-

Table 1
Physical parameters of catalyst layers based on Pt/OMC catalyst

Sample	LL_{Pt} (mg cm^{-2})	Ionomer content	Cathode compression	l_{cl} (μm)	ε_I	ε_C	ε_T	$\varepsilon_{I\text{-agg}}$
M18-U	2.39	0.18	×	70	0.029	0.117	0.854	0.250
M18-C	2.39	0.18	O	45	0.040	0.160	0.801	0.250
M30-U	2.64	0.30	×	128	0.029	0.071	0.900	0.416
M30-C	2.64	0.30	O	68	0.055	0.133	0.812	0.416
M45-U	2.39	0.45	×	132	0.039	0.062	0.900	0.624
M45-C	2.39	0.45	O	64	0.080	0.128	0.793	0.624

sis examining structural features such as ionomer volume fraction (ε_I), catalyst volume fraction (ε_C), total porosity (ε_T) and ionomer volume fraction in the agglomerate ($\varepsilon_{I\text{-agg}}$) is warranted. To generate binding of the catalyst and a continuous ion-conducing phase, ε_I should be higher than a certain level [27]. As reported by Boyer et al. [35], the ionic conductivity of the catalyst layer is correlated with the proton conductivity of ionomer by

$$\sigma_{cl} = \sigma_0 \varepsilon_I^n \quad (1)$$

where σ_{cl}, σ_0 and n are the ionic conductivity of catalyst layer, the ionic conductivity of the ionomer and an exponent that depends on the microstructure and tortuosity of the ionomer phase, respectively. Typical values of the exponent n are in the range from 1.2 to 4.5 [35–37]. From the theory of Bruggeman [37], the exponent equals 1.5. ε_C is based on the solid portion of Pt/OMC and can be regarded as the volume fraction of the electron-conducting medium. ε_T represents the portion of the space that is occupied by neither the electrolyte nor the catalyst. It includes mesopores within the OMC and macropores between the agglomerates. The pores in the catalyst layer act as a pathway for oxygen transport and by-product (water) transport and ε_T indicates the capability for mass transport. According to the agglomerate model [25,38], ionomer coats catalyst aggregates, forming a secondary particle. Oxygen should pass through the ionomer phase in the agglomerate to reach the catalyst surface to facilitate the oxygen-reduction reaction in this model. Also, water has to be removed from the catalyst surface and water diffusion through the ionomer phase in the agglomerate is included in the removal process. The oxygen and water diffusion through the agglomerate depends on the size of the agglomerate and on $\varepsilon_{I\text{-agg}}$. The thickness of ionomer layer covering catalyst particle increases with $\varepsilon_{I\text{-agg}}$ at a fixed agglomerate size. Therefore, $\varepsilon_{I\text{-agg}}$ is an important structural parameter relating to any diffusion process in the agglomerate. From the SEM images shown in Fig. 3, the agglomerate model appears to be appropriate to describe the Pt/OMC-based catalyst layers.

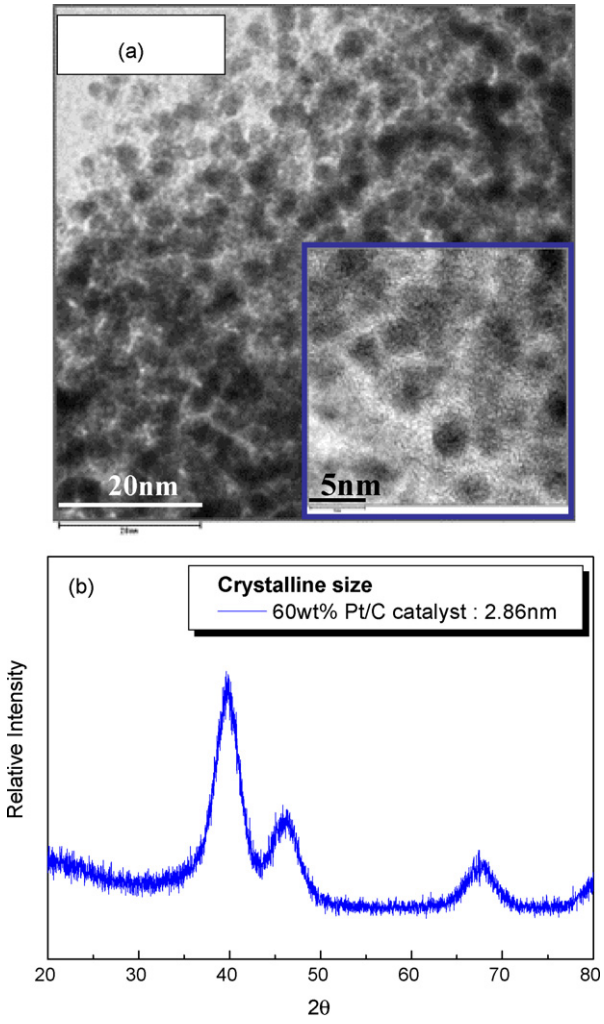

Fig. 2. (a) TEM image and (b) XRD pattern for Pt/OMC catalyst.

From the composition and thickness of the catalyst layer, ε_I, ε_C and ε_T were calculated using the following equations:

$$\varepsilon_I = \left(\frac{1}{\rho_I} \times R_I\right) \times \frac{LL_{Pt}}{l_{cl}} \quad (2)$$

$$\varepsilon_C = \left(\frac{1}{\rho_{Pt}} + \frac{1}{\rho_{OMC}} \times \frac{0.4}{0.6}\right) \times \frac{LL_{Pt}}{l_{cl}} \quad (3)$$

$$\varepsilon_T = 1 - \varepsilon_I - \varepsilon_C \quad (4)$$

where ρ_I, ρ_{Pt}, ρ_{OMC} and l_{cl} are the densities of the ionomer (Nafion®), Pt and OMC, and the thickness of catalyst layer, respectively. The values of ρ_I, ρ_{Pt} and ρ_{OMC} are 2.11, 21.4 and 2.26 g cm^{-3}, respectively. $\varepsilon_{I\text{-agg}}$ was also calculated from ε_I and ε_C as follows:

$$\varepsilon_{I\text{-agg}} = \frac{\varepsilon_I}{\varepsilon_C + \varepsilon_I} \quad (5)$$

The values of ε_I, ε_C, ε_T and $\varepsilon_{I\text{-agg}}$ are listed in Table 1. Increase in the ionomer content and the catalyst layer compaction lead to increase of ε_I. ε_T is little affected by the ionomer content, whereas it is considerably reduced by the compression. ε_C decreases with increase in ionomer content and increases with compression.

3.3. Relationship between structural parameters and power performance

Fig. 4 and Table 2 represent *I–V* characteristics on the fifth day at 50, 60 and 70 °C, and power densities at 0.45 V, respectively. The operating voltage was chosen considering a balance between power density and energy efficiency. Operation at lower voltage generates high power density, and thus size reduction of the stack is possible. On the other hand, energy efficiency decreases on lowering the voltage, which requires a larger fuel tank for a given energy consumption. As a result of the optimization to yield a smaller total system, an operating voltage of 0.45 V is chosen. Dry air and 1 M aqueous methanol solution were used as feedstocks for the cath-

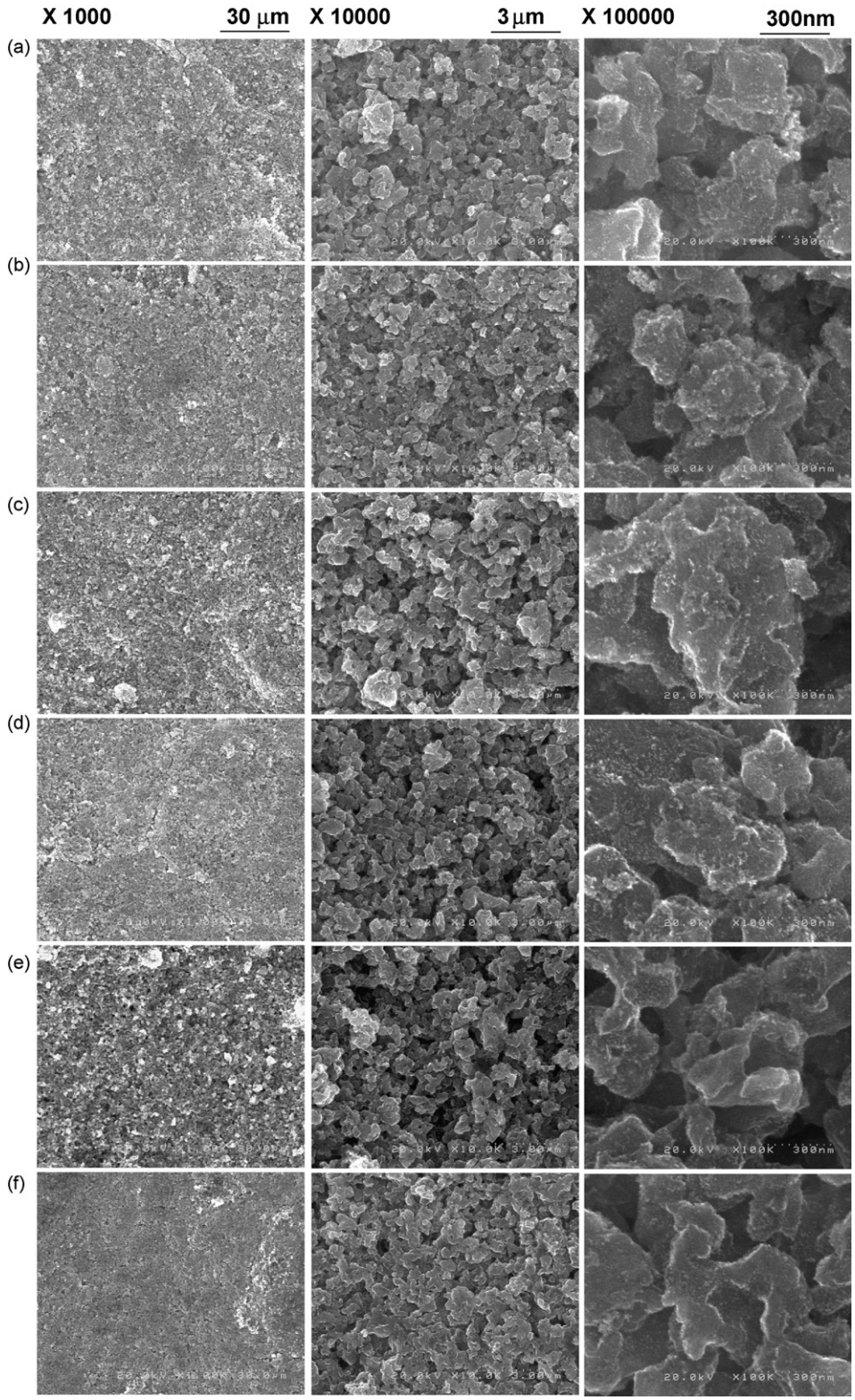

Fig. 3. SEM images of (a) M18-U, (b) M18-C, (c) M30-U, (d) M30-C, (e) M45-U and (f) M45-C (magnification: 1000× for figure on left-hand side, 10,000× for figure in centre and 100,000× for figure on right-hand side).

ode and the anode, respectively. At the temperatures measured, uncompressed MEAs show higher power density at 0.45 V than compressed MEAs at the same ionomer content. The change in the ionomer content results in a more pronounced change than compression, which is consistent with a previously reported result on a supported catalyst [39]. As indicated from the change in ε_T and the SEM images (Fig. 3), the catalyst layer becomes more compact after compression, which will reduce mass transport in the electrode. By contrast, the ionic conductivity in the catalyst layer (σ_{cl}) should increase with compression due to the increased ε_I, as shown by Eq. (1), which will be confirmed by the impedance analysis described in Section 3.4. The decrease in performance with the compression

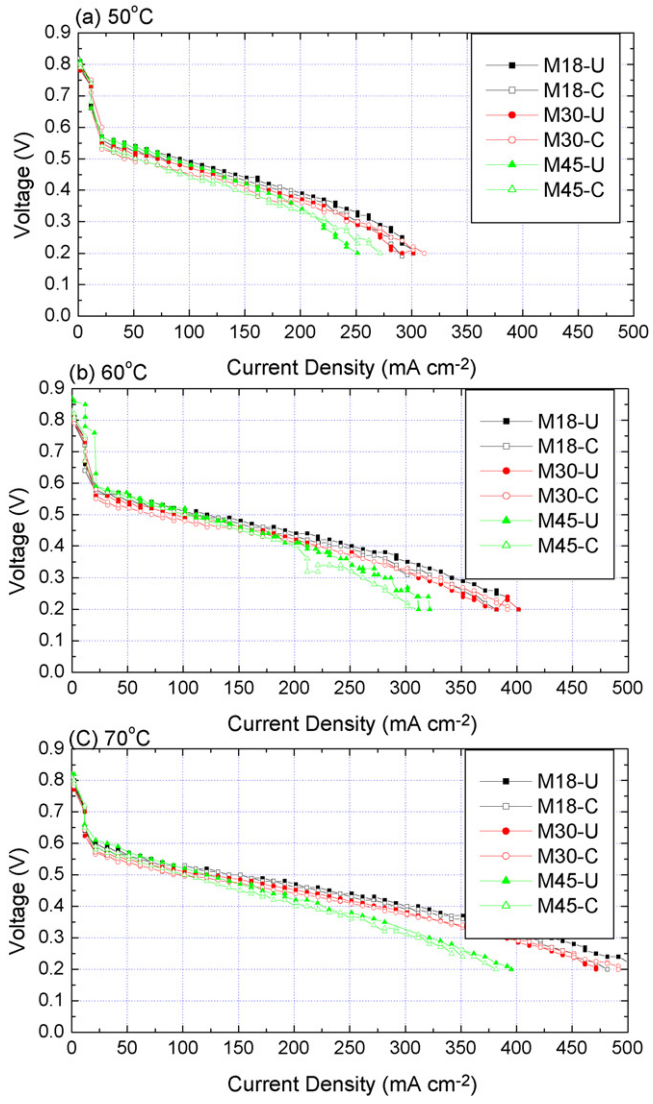

Fig. 4. *I–V* polarization for MEAs based on Pt/OMC catalyst at (a) 50 °C, (b) 60 °C and (c) 70 °C (cathode feed: air, anode feed: 1 M CH_3OH, stoichiometry for cathode: 3 and stoichiometry for anode: 3).

shows that mass transport is more important than ionic transport for the Pt/OMC-based catalyst layers. A similar finding was reported for a PtRu/C-supported catalyst based on Vulcan XC-72 [40]; the compaction of the anode catalyst layer led to a decrease in performance by 23% due to the increased mass-transport limitation.

For both the uncompressed and compressed series of MEAs, the power density increases with decrease in the ionomer content above 150 mA cm^{-2}. Below 150 mA cm^{-2}, however, the difference is less pronounced; the power density of M45-U appears to be comparable with that of M18-U. The large difference in power densities at high current densities indicates a considerable mass-transport limitation at high ionomer content.

Table 2
Power density at 0.45 V for Pt/OMC-based catalyst layers at 50, 60 and 70 °C

Sample	Power density at 0.45 V (mW cm^{-2})		
	50 °C	60 °C	70 °C
M18-U	64.0	86.2	104.2
M18-C	59.4	80.8	99.7
M30-U	54.9	76.3	91.1
M30-C	45.9	67.7	82.0
M45-U	56.7	68.2	77.5
M45-C	41.4	61.9	71.8

When conventional Pt-supported carbon is used, there is an optimum value of ionomer content in the catalyst layer to obtain the best performance [25]. Even though the existence of an optimum at lower ionomer content is expected for a Pt/OMC-based catalyst layer, it is not possible to confirm this because the mechanical integrity of the catalyst layer is not sufficient to obtain reliable data below an R_I of 0.18. An improvement in the formation of the three-dimensional network of the ionomer phase which provides mechanical integrity is needed to confirm the existence of an optimum at lower content of ionomer.

The relationship between the structural parameters of the catalyst layer and the power performance was investigated. Fig. 5 shows the changes in power density with ε_I, ε_C, ε_T and $\varepsilon_{I\text{-}agg}$. ε_I and ε_T are not correlated with the power density, as shown in Fig. 5(a) and (c), respectively. The increase in ε_C appears to enhance power density for both uncompressed and compressed samples. Nevertheless, the uncompressed and the compressed sample series exhibit a divided domain in the plot (Fig. 5(b)), which indicates that ε_C is not a decisive determinant of power performance. Interestingly, a strong correlation between $\varepsilon_{I\text{-}agg}$ and power density is observed, as displayed in Fig. 5(d). Both the uncompressed and compressed series show a decreasing tendency of power density with increase in $\varepsilon_{I\text{-}agg}$. The inverse relationship between $\varepsilon_{I\text{-}agg}$ and power performance suggests that the diffusion process through the ionomer phase in the agglomerate dominates the oxygen reduction reaction. With increase in $\varepsilon_{I\text{-}agg}$, the thickness of the ionomer phase covering the Pt/OMC agglomerate is also increased, which results in an increase in the diffusion path for oxygen and water. The gap in the power density between the compressed and uncompressed series would correspond to the effect of the contraction in macropores that is observed from SEM studies (see Fig. 3). From these analyses, it can be concluded that the mass-transport process governs the oxygen reduction reaction in the Pt/OMC-based cathode catalyst layer.

3.4. Impedance analysis of Pt/OMC cathode

The electrochemical characteristics of the catalyst layer were further investigated by means of electrochemical impedance spectroscopy. As described in Section 2, the cathode impedance was extracted from the total impedance. The total, anode and cathode impedances of M30-U are presented in Fig. 6. The ohmic resistance, which involves contributions from the membrane resistance and the electronic resistance, corresponds to the intercept in the high-frequency domain on the Z'-axis in the total impedance spectrum (Fig. 6(a)). The value for the ohmic resistance is 0.12 Ω cm^2 and shows no change with current density. The semi-circle in the middle-frequency region of the total impedance represents the fuel-cell reaction kinetics, with contributions from the cathodic oxygen-reduction process and the anodic methanol-oxidation process. At low frequencies, instability in impedance is observed, which means that the impedance fluctuates over a relatively long time-scale during the measurement. In general, the impedance at low frequency is related to a mass-transport process, which is the longest process occurring in the MEA. The anode impedance shown in Fig. 6(b) exhibits a typical feature of a methanol oxidation reaction; the size of the middle-frequency semi-circle decreases with current density, indicating faster electrochemical methanol oxidation. The cathode impedance obtained by subtracting the anode impedance from the total impedance (Fig. 6(c)) shows significant instability at low frequencies. Thus the instability in the total impedance is due to cathode performance.

The cathode impedance reveals a linear relationship between Z'' and Z' in the high-frequency region, as shown in Fig. 7(a). In this region, Faradaic processes are not significant; double-layer charg-

ing effects and proton transport through the catalyst layer dominate the overall electrode response which is typical of a porous electrode [27,41,42]. Accordingly, impedance can be expressed in terms of the ionic resistance (R_{cl}), double-layer capacitance (C_{dl}) of the cathode catalyst layer and frequency (ω) as follows:

$$|Z| = \sqrt{\frac{R_{cl}}{C_{dl}}}\omega^{-1/2} \quad (6)$$

The ratio of the ionic resistance and the double-layer capacitance is determined by fitting the linear region with Eq. (6). The double-layer capacitance is obtained from the capacitive charging current

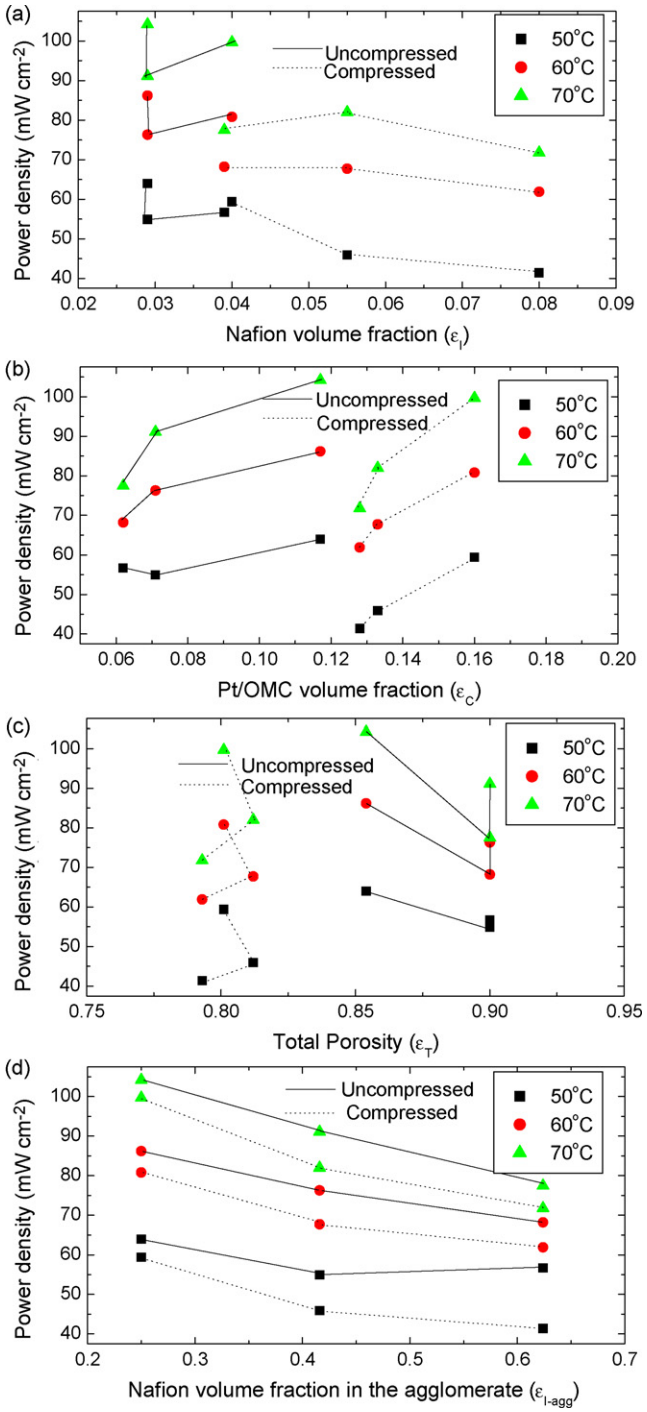

Fig. 5. Plot of power density at 70 °C and 0.45 V as function of (a) ε_l, (b) ε_C, (c) ε_T and (d) $\varepsilon_{l\text{-agg}}$.

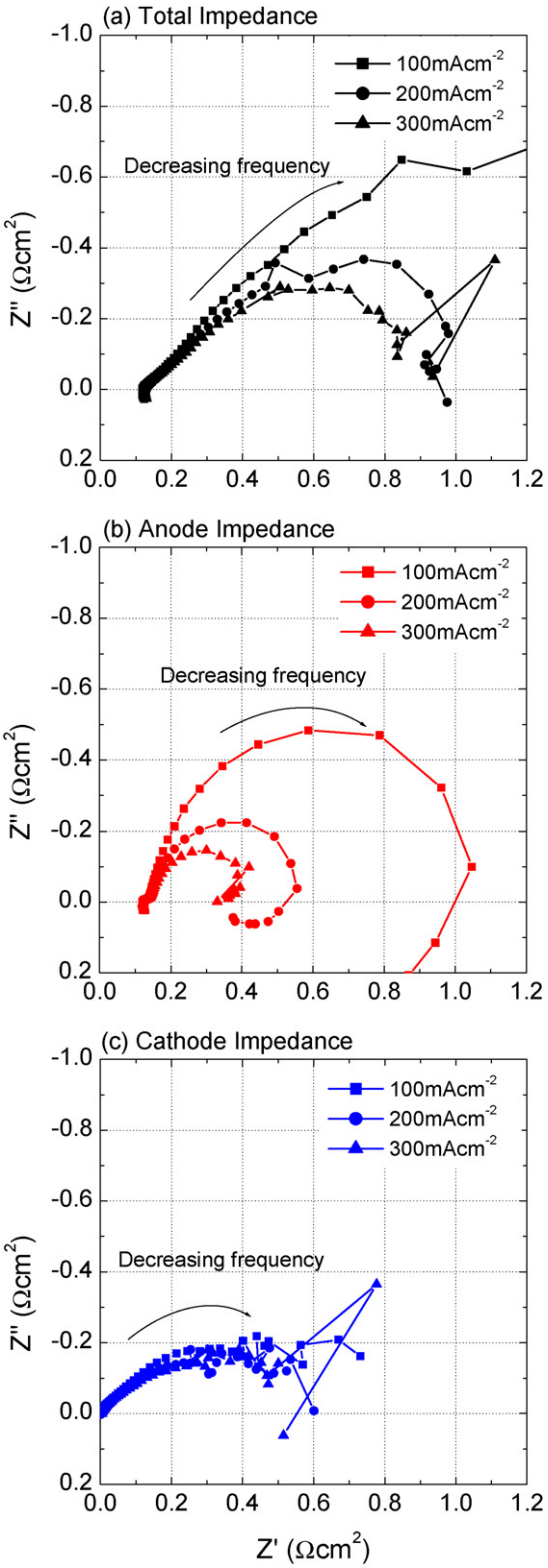

Fig. 6. Typical Nyquist plot of (a) total impedance, (b) anode impedance and (c) cathode impedance measured using M30-U at 70 °C.

of cyclic voltammograms, as described above. The ionic resistance is then calculated.

Values of the double-layer capacitance and the ionic resistance of the Pt/OMC-based catalyst layers at 70 °C are listed in Table 3 and are plotted as a function of ε_l in Fig. 7(b). The C_{dl} appears to show

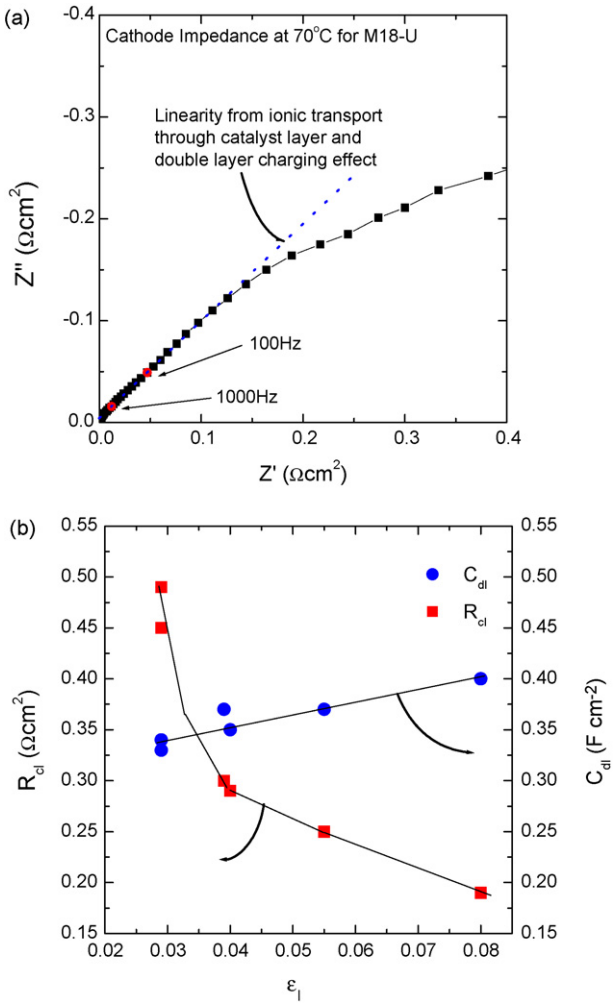

Fig. 7. (a) Linear region in Nyquist plot of cathode impedance for M30-U measured at 70 °C and (b) plot of ionic resistance and double-layer capacitance of Pt/OMC-based catalyst at 70 °C as function of ε_l.

a weak increase from 0.33 to 0.40 F cm^{-2} and R_{cl} decreases from 0.49 to 0.19 Ω cm^2. According to a previous report [27] on the effect of ionomer on the DMFC anode catalyst layer, the C_{dl} of the PtRu-black-based catalyst layer in the range of 0.16–0.21 F cm^{-2} with a PtRu loading of 1.4–2.3 mg cm^{-2} and the maximum occurs at an intermediate ε_l of approximately 0.08. Since Pt/OMC has a larger surface area than PtRu-black, a maximum in C_{dl} for Pt/OMC would be observed above an ε_l of 0.08. The value for ε_l in this investigation ranged from 0.053 to 0.08. The gradual decrease in R_{cl} with ε_l is obvious from Eq. (1).

In conjunction with the results shown in Fig. 5(d), the results given in Fig. 7(b) means that the best performance of the Pt/OMC cathodes is obtained at high-ionic resistance of the catalyst layer and vice versa. Hence, ionic conduction was less important for the performance of the cathode in the range of ε_l that is investigated. Compared with proton and electron conduction, the mass transport of oxygen/water is a decisive factor for the cathode performance.

Fig. 8 presents the impedance of the catalyst layers studied in this work measured at 70 °C and various current densities of 100, 200 and 300 mA cm^{-2}. At all the current densities, the cathode impedance is higher for higher ionomer contents. Comparing uncompressed and compressed MEAs, a difference is evident at high current density. At 100 mA cm^{-2}, compressed and uncompressed MEAs do not show any difference; at 200 and 300 mA cm^{-2}, however, the compressed MEA has a much higher impedance than the uncompressed MEA.

Table 3
Ionic resistance and double-layer capacitance at 70 °C for Pt/OMC-based catalyst layers

Sample	R_{cl} (Ω cm^2)	C_{dl} (F cm^{-2})
M18-U	0.45	0.33
M18-C	0.29	0.35
M30-U	0.49	0.34
M30-C	0.25	0.37
M45-U	0.30	0.37
M45-C	0.19	0.40

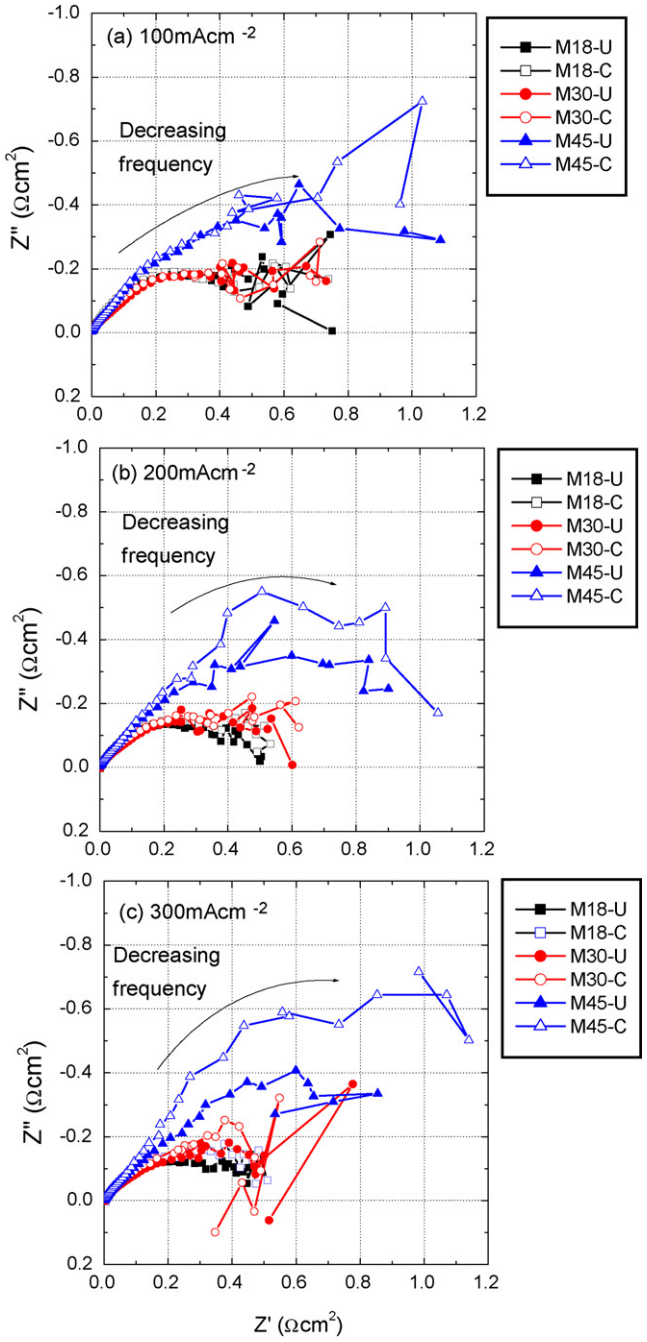

Fig. 8. Cathode impedance of Pt/OMC-based catalyst layers at 70 °C and at various current densities: (a) 100 mA cm^{-2}, (b) 200 mA cm^{-2} and (c) 300 mA cm^{-2}.

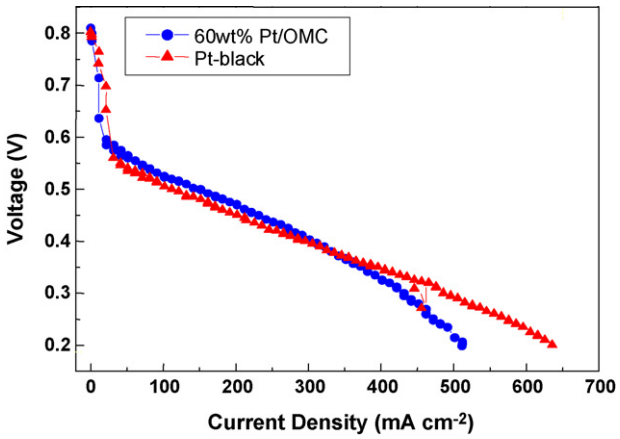

Fig. 9. Comparison of *I–V* polarization at 70 °C of Pt/OMC catalyst (6 mg cm^{-2}) and unsupported Pt-black (2 mg cm^{-2}) (cathode feed: air, anode feed: 1 M CH_3OH, stoichiometry for cathode: 3 and stoichiometry for anode: 3).

The instability at low frequencies becomes more significant with increase in ionomer content, which reconfirms a significant mass-transport limitation at high ionomer content, as expected from *I–V* polarization results. Local depletion of oxygen in the catalyst layer, due to the limited mass transport, may be responsible for the instability. Microscopic explanation for the mass-transport limitation can be made in terms of the pore structure of OMC. If the ionomer blocked the entrance or filled the inside of the mesopore, mass transport through the mesopore would be significantly limited. Mass-transport limitation for the OMC-based catalyst was also reported by Ding et al. [14]. A PtRu catalyst on a OMC was found to give unsteady behaviour during methanol oxidation at high current densities, and this behaviour was speculatively explained by the unsteady transport of reactants, intermediates and ions in the long narrow pores of the OMC.

3.5. Comparison of power performance of Pt/OMC-based and Pt-black-based catalyst layers

The *I–V* polarization behaviour of a M18-U catalyst layer at a loading level of 2 mg cm^{-2} and a catalyst layer based on Pt-black catalyst at a loading of 6 mg cm^{-2} is compared at Fig. 9. The thickness of the catalyst layer for the M18-U and Pt-black catalysts is 70 and 45 μm, respectively. The MEAs have identical components, except the cathode catalyst layer. The M18-U catalyst delivers higher power at high voltages (>0.4 V) and lower power density at low voltages (<0.4 V) than the Pt-black-based cathode. Since catalytic activity governs the electrochemical reaction rate at the high voltages (activation region), the higher power density for Pt/OMC indicates that 2 mg cm^{-2} of Pt/OMC gives higher catalytic activity than 6 mg cm^{-2} of Pt-black, which is of practical importance. With the introduction of an OMC support, the Pt loading in the cathode can be reduced to one-third of Pt-black-based catalyst layer, without any negative effect on power performance, and this would significantly contribute to cost reduction of MEAs. The lower power density for the Pt/OMC catalyst layer at high-current density indicates that the mass-transport limitation is greater than that for the Pt-black-based catalyst layer.

4. Conclusions

A high-performance catalyst layer based on a Pt/OMC catalyst has been developed. The observed power characteristics can be successfully described according to an agglomerate model. An increase in the Nafion® volume fraction in the agglomerate leads to a decrease in power performance, which indicates that it is not ionic transport through the catalyst layer but oxygen diffusion through the ionomer phase in the aggregate that governs the kinetics of oxygen reduction. A comparison of the uncompressed and the compressed catalyst layer indicates that macropores in the catalyst layer are also important for facile mass transport. Impedance spectroscopic investigations support this consideration. It is found that the optimum Pt/OMC catalyst layer with 2 mg cm^{-2} of platinum generates higher power than a conventional unsupported catalyst with 6 mg cm^{-2}.

References

[1] Z.R. Ismagilov, M.A. Kerzhentsev, N.V. Shikina, A.S. Lisitsyn, L.B. Okhlopkova, Ch.N. Barnakov, M. Sakashita, T. Iijima, K. Tadokoro, Catal. Today 58 (2005) 102.
[2] L. Zhang, B. Cheng, E.T. Samulski, Chem. Phys. Lett. 398 (2004) 505.
[3] M. Gangeri, G. Centi, A. La Malfa, S. Perathoner, R. Vieira, C. Phram-Huu, M.J. Ledoux, Catal. Today 50 (2005) 102.
[4] F. Yuan, H.K. Yu, H. Ryu, Electrochim. Acta 50 (2004) 685.
[5] N. Rajalakshmi, H. Ryu, M.M. Shujumon, S. Ramaprabhu, J. Power Sources 140 (2005) 250.
[6] W. Li, C. Liang, J. Qiu, W. Zhou, H. Han, Z. Wei, G. Sun, Q. Xin, Carbon 40 (2002) 787.
[7] H. Tang, J.H. Chen, Z.P. Huang, D.Z. Wang, Z.F. Ren, L.H. Nie, Y.F. Luang, S.Z. Yao, Carbon 42 (2004) 191.
[8] P. Kim, H. Kim, J.B. Joo, W. Kim, I.K. Song, J. Yi, J. Power Sources 145 (2005) 139.
[9] A. Smirnova, X. Dong, H. Hara, A. Vasiliev, N. Sammes, Int. J. Hydrogen Energ. 30 (2005) 149.
[10] J. Marie, S. Bretón-Fabry, P. Achard, M. Chatenet, A. Pradourat, E. Chainet, J. Non-Cryst. Solids 350 (2004) 88.
[11] P.V. Samant, C.M. Rangel, M.H. Romero, J.B. Fernandes, J.L. Figueiredo, J. Power Sources 151 (2005) 79.
[12] H. Chang, S.H. Joo, C. Pak, J. Mater. Chem. 17 (2007) 3078.
[13] J.-H. Nam, Y.-Y. Jang, Y.-U. Kwon, J.-D. Nam, Electrochem. Commun. 6 (2004) 737.
[14] J. Ding, K.-Y. Chan, J. Ren, F.-S. Xiao, Electrochem. Commun. 50 (2005) 3131.
[15] J.B. Joo, P. Kim, W. Kim, J. Kim, J. Yi, Catal. Today 111 (2006) 171.
[16] S.H. Joo, S.J. Choi, I. Oh, J. Kwak, Z. Liu, O. Terasaki, R. Ryoo, Nature 412 (2001) 169.
[17] S.H. Joo, C. Pak, D.J. You, S.-A. Lee, H.I. Lee, J.M. Kim, H. Chang, D. Seung, Electrochim. Acta 52 (2006) 1618.
[18] E.A. Ticianelli, C.R. Derouin, A. Redondo, S. Srinivasan, J. Electrochem. Soc. 135 (1988) 2209.
[19] Z. Poltarzewski, P. Staiti, V. Alderucci, W. Wieczareka, N. Giordano, J. Electrochem. Soc. 139 (1992) 761.
[20] M. Uchida, Y. Aoyama, N. Eda, A. Ohta, J. Electrochem. Soc. 142 (1995) 4143.
[21] S.J. Lee, S. Mukerjee, J. McBreen, Y.W. Rho, Y.T. Kho, T.H. Lee, Electrochim. Acta 43 (1998) 3693.
[22] J.M. Song, S.Y. Cha, W.M. Lee, J. Power Sources 94 (2001) 78.
[23] E. Passalacqua, F. Lufrano, G. Squadrito, A. Patti, L. Giorgi, Electrochim. Acta 46 (2001) 799.
[24] D. Song, Q. Wang, Z. Liu, M. Eikerling, Z. Xie, T. Navessin, S. Holdcroft, Electrochim. Acta 50 (2005) 3347.
[25] E. Antolini, L. Giorgi, A. Pozio, E. Passalacqua, J. Power Sources 77 (1999) 136.
[26] X. Zhao, X. Fan, S. Wang, S. Yang, B. Yi, Q. Xin, G. Sun, Int. J. Hydrogen Energ. 30 (2005) 1003.
[27] A. Havranek, K. Wippermann, J. Electroanal. Chem. 567 (2004) 305.
[28] J.-H. Kim, H.Y. Ha, I.-H. Oh, S.-A. Hong, H.N. Kim, H.-I. Lee, Electrochim. Acta 50 (2004) 801.
[29] V. Gogel, T. Frey, Z. Yongsheng, K.A. Friedrich, L. Jorissen, J. Garche, J. Power Sources 127 (2004) 172.
[30] L. Liu, C. Pu, R. Viswanathan, Q. Fan, R. Liu, E.S. Smotkin, Electrochim. Acta 43 (1998) 3657.
[31] T.V. Reshetenko, H.-T. Kim, H. Lee, M. Jang, H.-J. Kweon, J. Power Sources 160 (2006) 925.
[32] T.V. Reshentenko, H.-T. Kim, U. Krewer, H.-J. Kweon, Fuel Cells 7 (2007) 238.
[33] J.T. Muller, P.M. Urban, J. Power Sources 75 (1998) 139.
[34] J.T. Muller, P.M. Urban, W.F. Holderich, J. Power Sources 84 (1999) 364.
[35] C. Boyer, S. Gamburzev, O. Velev, S. Srinivasan, A.J. Appleby, Electrochim. Acta 43 (1998) 3703.
[36] M. Nakamura, J. Appl. Phys. 57 (1985) 1449.
[37] D.G. Bruggeman, J. Appl. Phys. 24 (1935) 636.
[38] M. Uchida, Y. Fukuoka, Y. Sugawara, N. Eda, A. Ohra, J. Electrochem. Soc. 143 (1996) 2245.
[39] Th. Frey, M. Linardi, Electrochim. Acta 50 (2004) 99.
[40] J. Zhang, G. Yin, Z. Wang, Y. Shao, J. Power Sources 160 (2006) 1035.
[41] M. Eikerling, A.A. Kornyshev, J. Electroanal. Chem. 475 (1999) 107.
[42] R. Makharia, M.F. Mathias, D.R. Baker, J. Electrochem. Soc. 152 (2005) A970.